

Transmission grid stability with large scale power flows due to renewables

María Martínez-Barbeito,* Damià Gomila, and Pere Colet
*Instituto de Física Interdisciplinar y Sistemas Complejos (IFISC, UIB-CSIC),
Campus Universitat de les Illes Balears E-07122, Palma de Mallorca, Spain*

Julian Fritzsche and Philippe Jacquod
*Department of Quantum Matter Physics, University of Geneva, CH-1211 Geneva, Switzerland and
School of Engineering, University of Applied Sciences of Western Switzerland HES-SO, CH-1950 Sion, Switzerland*
(Dated: November 30, 2023)

We propose a general methodology for identifying critical lines in the long-distance transmission of power across large electrical networks. When the system is pushed to its limits of operation due to large power imbalances or contingencies, the network may lose synchrony. We analyze the Continental Europe grid as a case study and find that instabilities emerge due to topological constraints by which the system loses its stable fixed point (synchronized state), causing the grid to split into two asynchronous zones. We discuss also how the modes of the system provide information on which areas are more susceptible to lose synchrony.

Keywords: power grid stability, renewable generation, long-distance power transmission, inter-area unbalances, critical power lines

I. INTRODUCTION

The steep increase in atmospheric and oceanic temperatures of the past decades is a direct consequence of anthropogenic emissions of greenhouse gases [1, 2]. Key to mitigating global warming is the strong reduction and, if at all possible, entire suppression of these emissions. Among the different greenhouse gases, carbon dioxide is of particular interest because of its emission volume and century-long lifetime in the atmosphere. Decarbonization – suppressing carbon dioxide emissions from human activities – is therefore crucial for climate change mitigation.

The energy sector is the main contributor to carbon dioxide emissions [3]. Thus, decarbonization requires a fundamental shift to low-carbon energy sources. Many countries have set as a goal to achieve climate neutrality by 2050 at the latest [4–7] as part of an international effort to combat climate change [8]. Achieving this goal requires substantial changes across various sectors of the economy and, in particular, transforming the energy sector. In upcoming years, the deployment of Variable Renewable Energy Sources (VRES) is expected to increase massively worldwide because of their lack of carbon emissions. Within Europe, for instance, electricity generation is expected to rely on an optimal combination of wind and solar power [9].

The integration of a large fraction of VRES in the power grid poses significant challenges [10, 11]. Their inherent variability and uncontrollable nature can lead to frequency and voltage fluctuations. Additionally, the transition from synchronous generators to a more electronics-based power system raises power quality issues [12–15]. Various alternatives have been proposed to

address these challenges. From storage systems [16], to power electronics that emulate inertia [17, 18], to inverters that mimic synchronous generators [19], a number of solutions have been proposed, each with its advantages and its shortcomings. Key aspects that need to be carefully taken into account are environmental and geographical factors restricting the deployment of VRES. Some regions possess greater renewable potential than others, hence they are likely to contribute more to the generation fraction. For instance, in Europe, Germany, Spain, France, and Italy, have the highest wind capacity plans [20]. VRES are both fluctuating and undispatchable, which will inevitably lead to local excess or lack of power supply. These can be significantly mitigated by large-scale power transfers over distant areas with different power mixes and varying meteorological conditions. Consequently, in parallel to decarbonization and the deployment of large quantities of VRES, there is a need for a grid infrastructure that supports large flows of energy across nations [21].

Large-scale high-voltage transmission grids result from the interconnection of national subsystems over decades and they were not originally designed to support large cross-border trades [22]. Moreover, national Transmission System Operators (TSOs) traditionally look after their own control area and exchange little real-time information with their counterpart in other interconnected areas. This makes the response to contingencies slower and inadequate, and the grid more prone to blackouts [23–27]. While the existing infrastructure and policies have improved in recent years [28], the expected cross-border exchanges may exceed the capacity of the current system design [29], which will push the system close to its limits.

It is therefore crucial to better understand how the upcoming large amounts of VRES will impact the legacy-power-system on which they will be deployed. This is the main focus of this article. Our goal is to analyze

* Corresponding author: maria@ifisc.uib-csic.es (she/her/hers)

grid stability in scenarios with large interregional power flows and identify which are the most vulnerable areas. The paper is structured as follows. Section II describes the dynamical model. Section III describes the European grid model on which we will focus and the methodology. In Sections IV and V, we present our results. Section VI summarises the main discussion points and concluding remarks. We stress that, while our numerical investigations focus on a model of the transmission grid of continental Europe, our conclusions apply to other, large-scale electric power grids.

II. MODEL

In the lossless line approximation and assuming constant voltage, the dynamics of a transmission grid can be described by the swing equation

$$m_i \ddot{\theta}_i + d_i \dot{\theta}_i = p_i + \sum_j b_{ij} \sin(\theta_j - \theta_i), \quad (1)$$

where θ_i is the voltage phase of bus i , for $i = 1, \dots, N$, m_i and d_i are its inertia and damping coefficients, p_i is the power generated (negative for net consumers), and $b_{ij} = B_{ij} V_{ij}^2$ is the theoretical maximum power flow for the transmission line between nodes i and j determined by its susceptance B_{ij} (imaginary part of the admittance) and voltage V_{ij} . As in [30], generator buses have inertia, $m_i > 0$, $i = 1, \dots, N_G$, while load buses are considered inertia-less, i.e., $m_i = 0$, $i = N_G + 1, \dots, N$.

The fixed points of (1) are given by $\theta_i^* = 0$ and $p_i^* + \sum_j b_{ij} \sin(\theta_j^* - \theta_i^*) = 0$. In what follows, we first revisit the stability analysis done in [31, 32] for the case in which all nodes have inertia. Then, we extend the results to the case in which there are inertia-less nodes.

In the case where all nodes have inertia, for given $\{p_i\}$, the stability of the fixed point is determined by the Jacobian

$$\mathbf{J} = \begin{bmatrix} \mathbf{0} & \mathbb{I} \\ -\mathbf{M}^{-1}\mathbf{L} & -\mathbf{M}^{-1}\mathbf{D} \end{bmatrix}, \quad (2)$$

where $\mathbf{M} = \text{diag}(m_1, \dots, m_N)$, $\mathbf{D} = \text{diag}(d_1, \dots, d_N)$, and \mathbf{L} is the network Laplacian defined as

$$\mathbf{L}_{ij} = \begin{cases} -b_{ij} \cos(\theta_i^* - \theta_j^*) & \text{for } i \neq j \\ \sum_k b_{ik} \cos(\theta_i^* - \theta_k^*) & \text{for } i = j \end{cases}. \quad (3)$$

The subscript ij denotes the rows (columns) corresponding to the i th (j th) node.

The eigenvalues of the Jacobian are given by

$$\left| \begin{array}{cc} -\Lambda \mathbb{I} & \mathbb{I} \\ -\mathbf{M}^{-1}\mathbf{L} & -\mathbf{M}^{-1}\mathbf{D} - \Lambda \mathbb{I} \end{array} \right| = 0, \quad (4)$$

hence

$$\left| -\Lambda(-\mathbf{M}^{-1}\mathbf{D} - \Lambda \mathbb{I}) + \mathbf{M}^{-1}\mathbf{L} \right| = 0. \quad (5)$$

This equation has a simple solution if the damping of the nodes is proportional to their inertia, namely

$$\frac{d_i}{m_i} = \kappa, \quad i = 1, \dots, N. \quad (6)$$

In this case, (5) becomes

$$\left| \Lambda(\kappa + \Lambda) \mathbb{I} + \mathbf{M}^{-1}\mathbf{L} \right| = 0. \quad (7)$$

Defining $\lambda = -\Lambda(\kappa + \Lambda)$, this is the eigenvalue equation for the matrix $\mathbf{M}^{-1}\mathbf{L}$. Thus, the eigenvalues of the Jacobian come in pairs: for each eigenvalue λ_i ($i = 1, \dots, N$) of $\mathbf{M}^{-1}\mathbf{L}$, we have two eigenvalues of the Jacobian given by

$$\Lambda_i^\pm = \frac{-\kappa \pm \sqrt{\kappa^2 - 4\lambda_i}}{2}. \quad (8)$$

In general, $\mathbf{M}^{-1}\mathbf{D}$ is not proportional to the identity matrix despite being diagonal. Therefore, (5) can not be solved easily. Nevertheless, it is possible to gain some insight from the Jacobian eigenvector equation. The phase, \vec{u}_j , and frequency, \vec{w}_j , components of the eigenvector \mathbf{j} ($j = 1, \dots, 2N$) fulfill

$$\mathbf{J} \begin{bmatrix} \vec{u}_j \\ \vec{w}_j \end{bmatrix} = \Lambda_j \begin{bmatrix} \vec{u}_j \\ \vec{w}_j \end{bmatrix}. \quad (9)$$

Thus,

$$\vec{w}_j = \Lambda_j \vec{u}_j, \quad (10)$$

$$-\mathbf{L} \vec{u}_j - \Lambda_j \mathbf{D} \vec{u}_j = \Lambda_j^2 \mathbf{M} \vec{u}_j. \quad (11)$$

Multiplying the left hand side by \vec{u}_j^\dagger and defining $a_j = \vec{u}_j^\dagger \mathbf{M} \vec{u}_j$, $b_j = \vec{u}_j^\dagger \mathbf{D} \vec{u}_j$, and $c_j = \vec{u}_j^\dagger \mathbf{L} \vec{u}_j$, we get

$$a_j \Lambda_j^2 + b_j \Lambda_j + c_j = 0, \quad (12)$$

as in [31]. Since $j = 1, \dots, 2N$, in principle, there are $4N$ solutions for Λ fulfilling (12), twice the number of actual eigenvalues. In fact, this derivation from the eigenvector equation provides a necessary condition for the eigenvalues but not a sufficient one, namely, not all solutions to (12) are eigenvalues. In the simple case where node damping is proportional to inertia, we can see that Eq. (11) for the phase components of the eigenvector associated to Λ^+ is identical to that for those associated to Λ^- . The eigenvectors differ in the frequency components. Therefore, there are only N values for coefficients a_i , b_i , and c_i , and no spurious solutions of (12).

Now, we focus on the case in which consumer nodes are inertia-less. The Jacobian is given by

$$\mathbf{J} = \begin{bmatrix} \mathbf{0} & \mathbf{0} & \mathbb{I} \\ -\mathbf{D}_{LL}^{-1} \mathbf{L}_{LG} & -\mathbf{D}_{LL}^{-1} \mathbf{L}_{LL} & \mathbf{0} \\ -\mathbf{M}_{GG}^{-1} \mathbf{L}_{GG} & -\mathbf{M}_{GG}^{-1} \mathbf{L}_{GL} & -\mathbf{M}_{GG}^{-1} \mathbf{D}_{GG} \end{bmatrix}, \quad (13)$$

with G (L) referring to the generator (load) variables. The Jacobian eigenvectors fulfill

$$\mathbf{J} \begin{bmatrix} \vec{u}_{Gj} \\ \vec{u}_{Lj} \\ \vec{w}_{Gj} \end{bmatrix} = \Lambda_j \begin{bmatrix} \vec{u}_{Gj} \\ \vec{u}_{Lj} \\ \vec{w}_{Gj} \end{bmatrix}, \quad (14)$$

where \vec{u}_{Gj} and \vec{u}_{Lj} are the generators' and consumers' phase components of the eigenvector j ($j = 1, \dots, N + N_G$), and \vec{w}_{Gj} are the generators' frequency components. This implies

$$\vec{w}_{Gj} = \Lambda_j \vec{u}_{Gj}, \quad (15)$$

$$- \mathbf{L}_{LG} \vec{u}_{Gj} - \mathbf{L}_{LL} \vec{u}_{Lj} = \Lambda_j \mathbf{D}_{LL} \vec{u}_{Lj} \quad (16)$$

$$- \mathbf{L}_{GG} \vec{u}_{Gj} - \mathbf{L}_{GL} \vec{u}_{Lj} - \Lambda_j \mathbf{D}_{GG} \vec{u}_{Gj} = \Lambda_j^2 \mathbf{M}_{GG} \vec{u}_{Gj}. \quad (17)$$

Defining $\mu_j = \vec{u}_{Lj}^\dagger \mathbf{D}_{LL} \vec{u}_{Lj}$ and $\nu_j = \vec{u}_{Lj}^\dagger \mathbf{L}_{LG} \vec{u}_{Gj} + \vec{u}_{Lj}^\dagger \mathbf{L}_{LL} \vec{u}_{Lj}$, from (16), we obtain the following linear equation for eigenvalues

$$\Lambda_j = -\frac{\nu_j}{\mu_j}. \quad (18)$$

Note that these eigenvalues depend mainly on the damping. The dependence on inertia comes only indirectly through the shape of the eigenvector. From (17), we get a quadratic equation for eigenvalues with strong dependence on inertia

$$\alpha_j \Lambda_j^2 + \beta_j \Lambda_j + \gamma_j = 0, \quad (19)$$

with $\alpha_j = \vec{u}_{Gj}^\dagger \mathbf{M}_{GG} \vec{u}_{Gj}$, $\beta_j = \vec{u}_{Gj}^\dagger \mathbf{D}_{GG} \vec{u}_{Gj}$, and $\gamma_j = \vec{u}_{Gj}^\dagger \mathbf{L}_{GG} \vec{u}_{Gj} + \vec{u}_{Gj}^\dagger \mathbf{L}_{GL} \vec{u}_{Lj}$.

The dynamical system (1) always has one zero eigenvalue due to the phase symmetry: adding the same constant value to all phases does not change the dynamics. The phase components of the eigenvector associated to this mode are given by $\vec{u}_0 = 1/\sqrt{N}[1, 1, \dots, 1]^T$, while the frequency components are $\vec{w}_0 = \vec{0}$. Since $\mathbf{M}^{-1}\mathbf{L}$ is a zero row sum matrix, \vec{u}_0 is an eigenvector with $\lambda_1 = 0$.

For the simple case where (6) is fulfilled, Eq. (8) for $\lambda_1 = 0$ leads to $\Lambda_1^+ = 0$ and $\Lambda_1^- = -\kappa$, which are the Jacobian neutral eigenvalue and the ratio of damping to inertia respectively. The eigenvector associated to Λ^- is $(\vec{u}, \vec{w}) = 1/\sqrt{N(1+\kappa)}[1, \dots, 1, -\kappa, \dots, -\kappa]^T$. For the general case where (6) is not fulfilled, there will not be an eigenvalue equal to $-\kappa$. Conventional power plants typically have inertia and damping proportional to their nominal capacity, although the proportionality coefficient depends on the plant technology. Besides, low inertia or inertia-less consumer nodes typically have a rather small damping. Therefore, while actual grids do not fulfill (6), eigenvalues and eigenvectors are relatively close to those encountered in the simple case.

The fixed points can only be created or lost through a saddle-node (SN) bifurcation, when a second eigenvalue of the Jacobian matrix vanishes [31, 32]. Since \mathbf{M} and \mathbf{D} are diagonal and positive, $a, b, \mu, \alpha, \beta > 0$. Therefore, the second zero eigenvalue of the Jacobian must be associated to $c_j = 0$, if all nodes have inertia, or to $\nu_j = 0$ or $\gamma_j = 0$, if consumers are inertia-less. In any case, this comes from a second zero eigenvalue of \mathbf{L} .

As shown in [33] (Lemma 2.8), for a connected weighted graph, a second eigenvalue of \mathbf{L} vanishes when

$$\sum_T \pi(T) = 0, \quad (20)$$

where the sum runs over all spanning trees T of the graph, and

$$\pi(T) = \prod_{(i,j) \in T} L_{ij}. \quad (21)$$

The sum cannot vanish if all edge weights $b_{ij} \cos(\theta_j^* - \theta_i^*)$ are positive. However, as soon as a line l_s reaches a $\pi/2$ phase difference, $\pi(T) = 0$ for all spanning trees including l_s . There are two scenarios: a) If l_s is the unique line connecting a part of the grid with the rest (for instance a leaf node of a cul-de-sac configuration), it is part of all spanning trees and thus all terms of the sum become zero simultaneously. There is grid separation into two areas and the frequency in one area deviates from the one in the other area, destroying the fixed point. This is similar to when a graph becomes disconnected [34]. b) If l_s is not the unique line connecting a part of the grid to the rest, its phase difference can be larger than $\pi/2$. Then, $\pi(T) < 0$ for all the spanning trees including l_s . At some point this can lead to the sum being zero, triggering an instability. This explains how stability is lost when one or several phase differences exceed $\pi/2$.

For the very unlikely case of two or more lines reaching simultaneously a $\pi/2$ phase difference, scenario a) applies if all the lines connecting a part of the grid with the rest are within the set of lines that have reached $\pi/2$. Otherwise, scenario b) applies.

Typically, the nominal capacity of a line is first restricted by its thermal limit, which is often much lower than the maximum flow b_{ij} . Transmission power grids are designed to operate normally at phase differences smaller than $\pi/4$. Therefore, regimes where phase differences are close to $\pi/2$ cannot be sustained for long periods of time. However, large phase differences can be reached during transients. It is important to maintain the stability of the power grid under these conditions to avoid the loss of synchrony during a contingency.

III. IMBALANCES IN THE EUROPEAN GRID

We apply the previous analysis to a large heterogeneous grid, where instabilities are generally not associated to line overloads. In particular, we consider PanTaN-GruEl [30, 35], an Open-Access model [36] for the synchronous grid of continental Europe. It considers a total of $N = 3809$ buses, of which $N_G = 468$ are operative generators, and 4944 power lines. Inertia, damping, and line parameters are heterogeneous. The generation and load of each bus is obtained with an optimal power flow using publicly available data from ENTSO-E [37]. Therefore, this is a realistic representation of the actual grid.

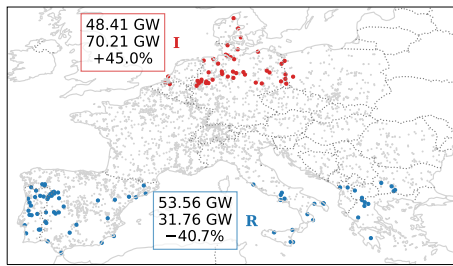


FIG. 1. Blue and red dots mark generators where power is reduced (R) and increased (I) respectively. Each text box displays the initial, final, and percentage change in generation of the marked nodes.

In the next sections, we analyze how increasingly large generation imbalances between different regions affect the stability of the grid. We focus on the power balance only, assuming there is enough control capacity. We explore various generation distributions, all derived from a reference dispatch. The reference dispatch is obtained using the optimization algorithm described in [36]. This algorithm calculates the generation and the load at each node from ENTSO-E load data at country level for a specific date and time. Then, to obtain the different generation configurations, we reduce the generation in region R by a fraction r and increase it in region I by i such that the total generation remains unchanged.

The reference dispatch is a fixed point of the system. If we modify the generation distribution, the power flow will also change. Thus, we have to calculate the new fixed points of the system for each new generation configuration. Using Newton’s method, we calculate and continue the fixed point for increasing values of r . Then, we analyze the linear stability of the fixed point by computing the eigenvalues and eigenvectors of the Jacobian matrix evaluated at that point.

IV. NORTH-SOUTH IMBALANCES

The North of Europe is witnessing a significant growth in wind power generation, both onshore and offshore. Countries such as Denmark, Germany, and the Netherlands, have favorable geographical conditions for strong and consistent winds, which make these areas prime locations for wind farms. Conversely, the South of Europe has ideal conditions for photovoltaic generation. For this reason, we explore scenarios where the generation increases in the Northern regions and decreases below a specific latitude, and vice versa. We present the results for the case shown in FIG. 1.

FIG. 2(a) shows the least damped eigenvalues obtained from a linear stability analysis of the reference case. The real eigenvalue arising from the neutral phase eigenvector of the Jacobian, $\Lambda = 0$, and the one with an eigenvalue close to $\Lambda = -\sum d_i / \sum m_i = -0.339$ are plotted in yellow and green respectively. There are an additional

3351 real eigenvalues which come from phase eigenvectors with tiny components in the generator nodes, $\bar{u}_{G_j} \approx 0$. These are given by (18). They are more damped, hence they are located to the left of the figure. The remaining $2(N_G - 1) = 914$ eigenvalues are complex and have relatively small damping, given by $-\beta_j/2\alpha_j$, and they are all shown in the figure.

In FIG. 2, we also take a closer look at some relevant modes. All eigenvectors have a phase component for each bus and a frequency component for each generator. On one hand, panels (b) and (c) show the frequency components of the lowest frequency mode, i.e., magenta and lilac eigenvalues in panel (a). We plot modulus and phase because this is a complex mode, hence it has imaginary components. We observe that this mode has a large constant amplitude in the Iberian Peninsula and the Balkans, while it is zero in Central Europe. Thus, when it is excited, it creates large antiphase coherent oscillations between east and west. These oscillations are known in the literature as inter-area oscillations [38]. This mode is associated with the least damped mode of the Laplacian. However, it is not the least damped mode of the Jacobian due to the heterogeneous distribution of inertia and damping across the network. Although not shown here, the frequency components are similar to the phase components.

On the other hand, panels (d) and (e) show the phase components of two of the least damped real modes. Since they are real, the eigenvectors only have real components. These two modes in particular are localized in Madrid and in the French Atlantic Coast, which are areas with several consumer buses but very few generators. In fact, the projection of the inertia matrix on these modes is very small. Their frequency component is also very small throughout the network except in the few generators close to these locations, which determine the response to frequency fluctuations. Although we only show these two modes in particular, the discussion is general for all real modes.

As the power imbalance increases, the system loses stability through a SN bifurcation at $r^* = 0.40703$. While this bifurcation involves a real eigenvalue reaching zero, it does not come from any of the real eigenvalues given by (18) with small components on nodes with inertia. Rather, the scenario is as shown in FIG. 3. For a pair of complex conjugate eigenvalues, the imaginary part decreases until it becomes zero and the eigenvalues become real. This is a Belyakov-Devaney transition (BD) [39, 40]. The two resulting real eigenvalues move away from each other. One moves towards negative values, while the other moves towards positive values, causing the SN bifurcation when reaching zero. Since eigenvalues separate very fast after the BD, in parameter space, the SN bifurcation is located very close to the BD.

In panels (a) and (b) of FIG. 4, we show the eigenvector associated with the eigenvalue that reaches zero. Note that, initially, this mode was as in FIG. 2(b) and 2(c). As the interarea power imbalance increases, the

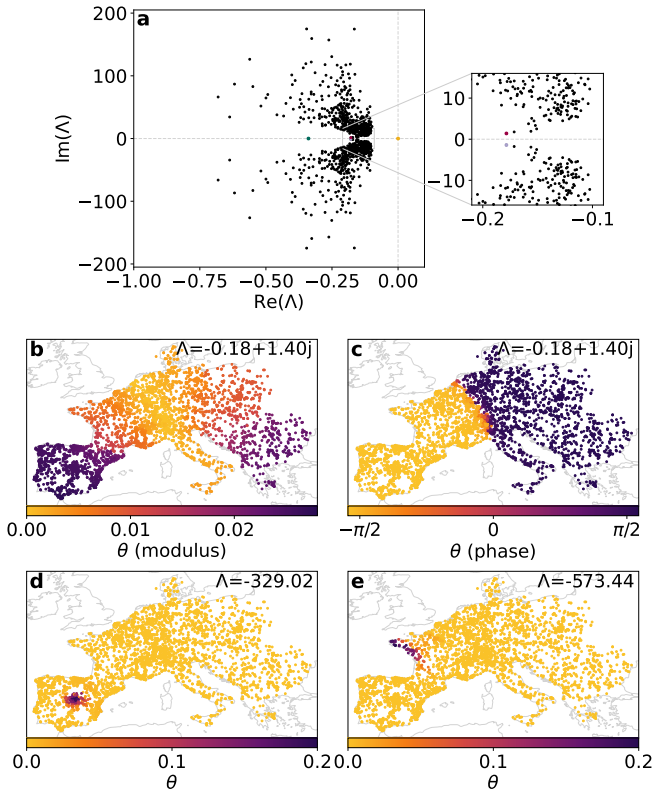


FIG. 2. (a) Least damped eigenvalues for the reference case. Phase components of some eigenvectors: (b,c) lowest frequency, (d) second and (e) third least damped real modes.

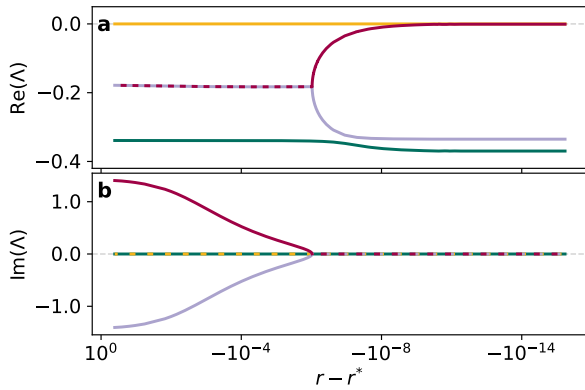


FIG. 3. Evolution of the (a) real and (b) imaginary parts of the zero eigenvalue (yellow), least damped real one (green), and the complex conjugate pair (lilac and magenta) involved in the BD transition and triggering the SN bifurcation. The horizontal axis is plotted in logarithmic scale with respect to the value r^* at which the SN bifurcation takes place.

mode changes, showing that the grid splits into two areas when the system reaches instability. Although the generation increases in the North, the splitting does not occur around the region where the power increases. The power is carried from that area to elsewhere, causing large power flows throughout the grid. Spain and Por-

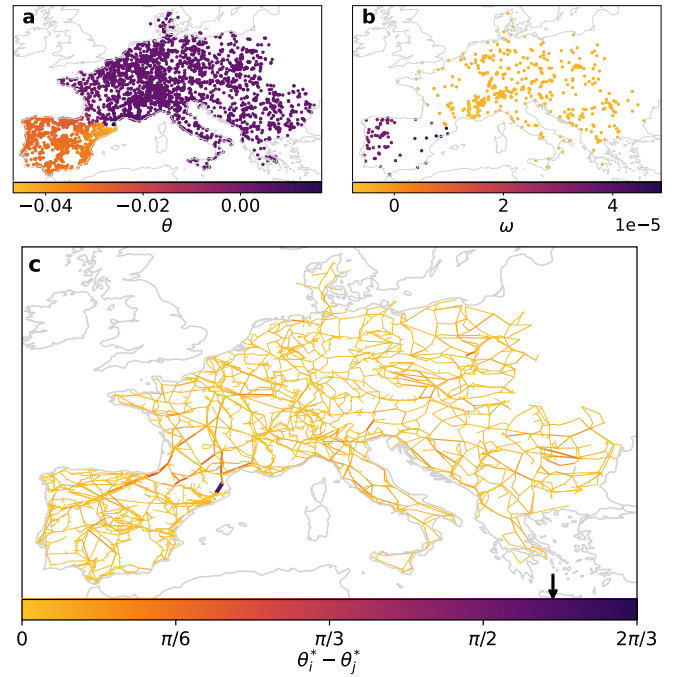


FIG. 4. (a) Phase and (b) frequency components of the eigenvector associated with the eigenvalue that reaches zero at the SN. (c) Line phase differences at the threshold of instability. The arrow in the color scale signals the maximum phase difference.

tugal, given their geographical location in the Iberian peninsula, have limited connectivity to France and the rest of the grid. This area is known to be a bottleneck of the European grid. In fact, the Iberian Peninsula has been historically considered an electric island [41].

In panel (c) of FIG. 4, we show the phase differences of the lines just before the SN bifurcation. We observe that the phase difference of one of the four lines between Spain and France is above $\pi/2$. For a $\pi/2$ phase difference, the line flow is maximum. Beyond $\pi/2$, the flow carried by the line decreases as the phase difference increases. Hence, the other lines have to carry more flow to compensate. The instability takes place when the flow carried by the lines is not enough to fulfill the needs in the Iberian Peninsula. It is not due to a capacity saturation, but to a restriction on the phase differences. Thus, the problem does not lie in having insufficient transmission capacity, but rather in the topology of the grid itself.

More specifically, for the reference case, the power imbalance in the Iberian Peninsula is -2.92 GW. It is negative because the demand is higher than the generation in the territory, hence it needs to import power from France and the rest of the grid. At the threshold of the instability, the power imbalance has been increased to -14.92 GW. At that point, the line *Baixas 380 - Vic 380* has a phase difference of 103.6° , i.e., it is at 97.2% of its capacity. For the other three lines, the phase difference is below 0.77 and the flow is less than 70% the maxi-

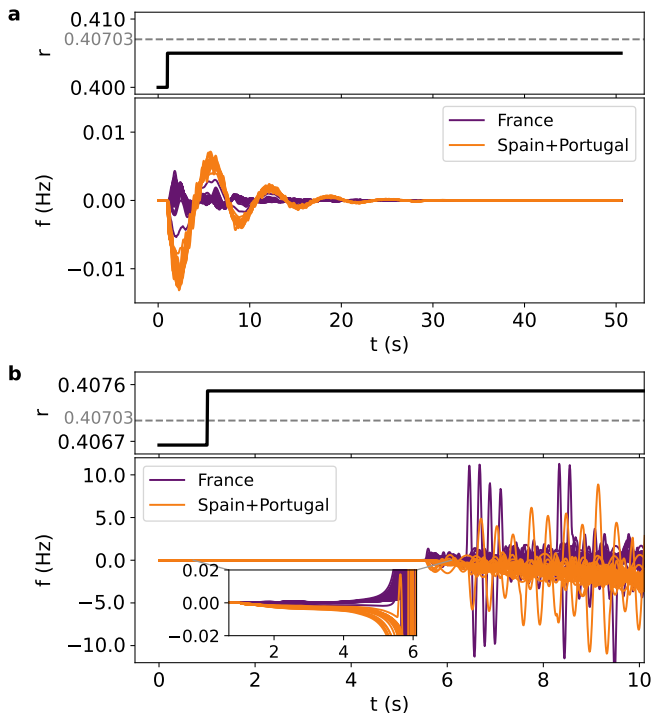


FIG. 5. Frequency of generators in Spain and Portugal (orange lines) compared to those in France (purple lines) after increasing, at time $t = 1$ s, the imbalance ratio r to (a) a value below or (b) above r^* .

imum. In total, these four lines are transmitting 14.92 GW, which is the required power needed to balance demand and generation in the territory, while their total transmission capacity is 20.74 GW.

To further illustrate what is happening close to the instability, we also run simulations of the dynamics. In FIG. 5, starting simulations from a fixed point at r below the critical value r^* , we increase r and let the system evolve. In panel (a), the final value for r is still below r^* , hence the system reaches a new fixed point after a short transient. However, in panel (b), where r is above the critical value, the system does not reach a new fixed point. In the initial seconds, the frequency decreases for the nodes in the Iberian peninsula. As shown in the inset, this causes the system to split into two unbalanced asynchronous areas. Finally, the frequency reaches an incoherent state with very large oscillations.

Splitting in the Pyrenees occurs also in other scenarios that entail large power flows between the Iberian Peninsula and other regions. For instance, we have also analyzed an scenario where generation decreases in Spain and Portugal, while it increases in France. The instability mechanism is the same as before, with the same unstable eigenvector, and takes place when the lines in the Pyrenees carry 14.91 GW. The line *Baixas - Vic* is at 97.2% of its capacity, while all others are below 69.3%. Similar results hold if we randomize the reduction or increase in generation at different nodes within a selected

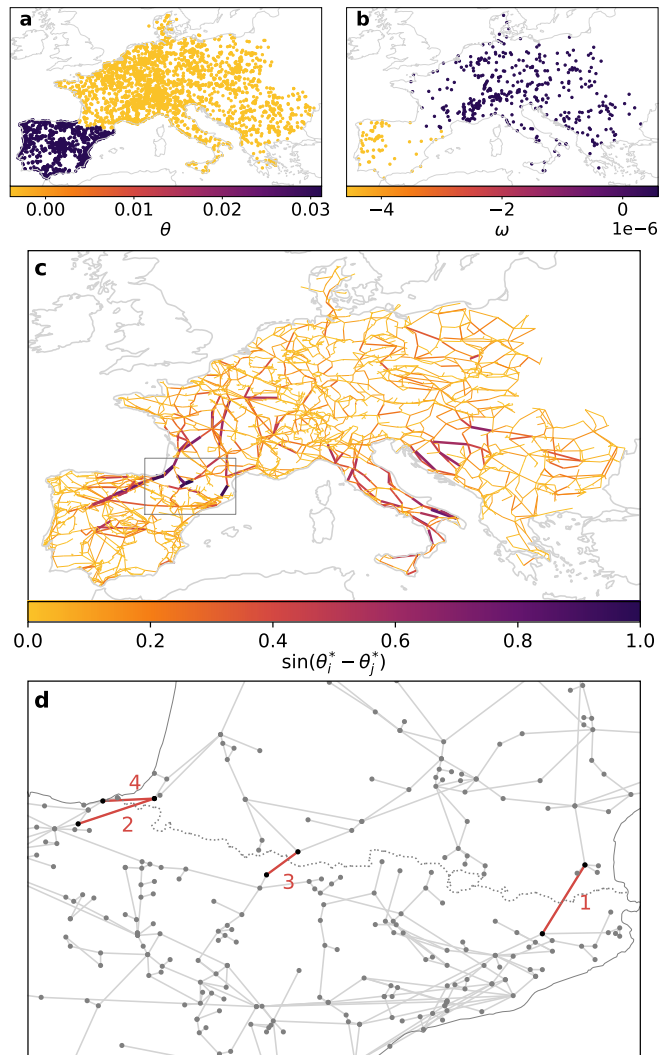


FIG. 6. (a) Phase and (b) frequency components of the eigenvector associated with the eigenvalue that becomes zero; (c) line stress at the threshold of the instability; and (d) lines changed to DC in the splitting region labeled by order of conversion.

region. The values may change slightly, but the behavior remains the same. We note, however, that if the North-South separation is moved much to the North, beyond parallel 50, the instability may take place first in the Balkans, similarly to that described in Section V.

The instability is dictated by topology constraints imposed by the fact that the power transmitted by alternating current (AC) lines depends on the phase difference between the connected buses. Contrary to AC lines, the power carried by direct current (DC) lines does not depend on such phase difference. With this in mind, we propose a method to stabilize the system beyond the instability observed with AC lines. The method is to be applied to the lines that reach phase differences larger than $\pi/2$ and it works as follows: for phase differences smaller than $\pi/2$, the line operates as a regular AC line, i.e., the

power flow is proportional to the $\sin(\theta_j - \theta_i)$. However, for phase differences beyond $\pi/2$, the flow remains the maximum one, i.e., b_{ij} in the model, no matter the phase of the connecting buses. Such mathematical trick could be implemented using HVDC lines, where the power electronics of converters can be programmed to deliver any desired power. Beyond its practical implementation, theoretically, this method allows us to identify the critical lines that separate two synchronous regions. By extending the existence of the fixed point, the lines that progressively reach a $\pi/2$ phase difference indicate a natural segmentation of the grid.

Redefining for $i \neq j$

$$L_{ij} = \begin{cases} b_{ij} \cos(\theta_j - \theta_i) & \text{for } |\theta_j - \theta_i| \leq \pi/2 \\ 0 & \text{for } |\theta_j - \theta_i| > \pi/2 \end{cases}, \quad (22)$$

the stability analysis discussed in Section II holds. In particular, instability takes place when (20) is fulfilled. The difference is that now $L_{ij} \geq 0$, thus instabilities can only take place via scenario a). As a consequence, applying this method, the fixed point is more robust and can be continued for larger generation imbalances. In particular, for the case illustrated in FIG. 1, from 40.7% to 60.4%, which is the point where all interconnections between Spain and France reach their maximum capacity. After that, the grid clearly separates into two asynchronous zones, as shown in panels (a) and (b) of FIG. 6.

In panel (c), we show the stress of lines at the threshold of the instability. Note that this is the last stable state of the system before line 4 reaches a $\pi/2$ phase difference. When that happens, the network separates into two components and the Jacobian matrix will have a new zero eigenvalue. Since Newton's method cannot handle singular matrices, convergence stops.

Finally, in panel (d), we zoom into the Pyrenees region, where HVDC lines are displayed in red and labeled according to order in which they have reached a phase difference of $\pi/2$ and become controlled. We can see that the Iberian Peninsula would completely disconnect from the rest of the grid by removing those red links. Hence, it becomes asynchronous by changing those lines from AC to controlled HVDC.

V. CENTRAL-WEST IMBALANCES

The grid in the Balkan region is vulnerable due to historical reasons [42]. In 2021, many lines in that area overloaded during a situation of high power flows. This situation was caused by a lower demand in this region and a higher demand in Central and Western Europe due to weather conditions. This caused large power flows from South-East to North-West Europe, splitting the grid in two [43]. To replicate the 2021 situation, we reduce the generation in Central Europe, while simultaneously increasing it in the Balkan region, as shown in FIG. 7.

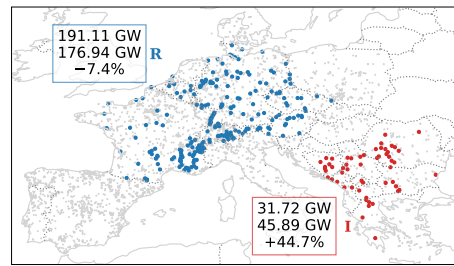


FIG. 7. Blue and red dots mark generators where power is reduced (R) and increased (I) respectively. Each text box displays the initial, final, and change in generation of the marked nodes.

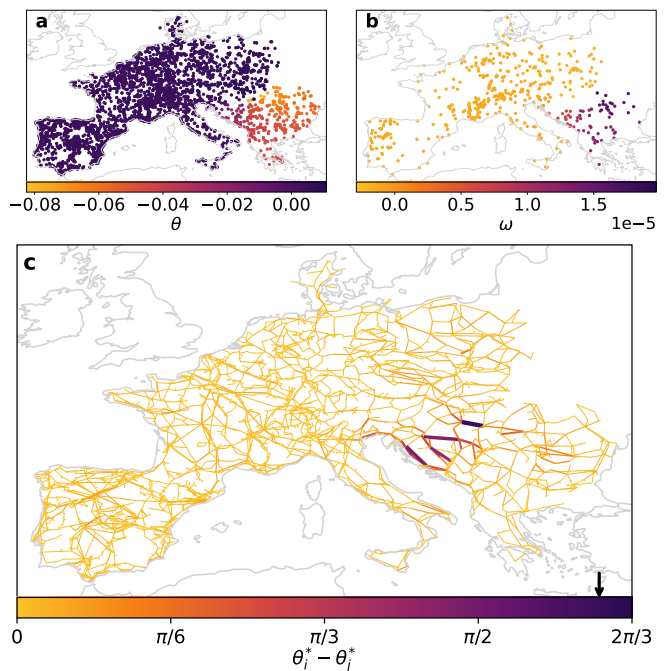


FIG. 8. (a) Phase and (b) frequency components of the eigenvector associated with the eigenvalue that crosses zero. (c) Phase difference at the fixed point at the threshold of instability. Arrow marks the maximum phase difference. Results for the case shown in FIG. 7.

After decreasing the generation by 7.4% in Central Europe, the grid splits. The instability scenario is similar to that described in Section IV. A pair of damped complex eigenvalues undergoes a BD leading to two real eigenvalues moving away from each other, with the largest triggering a SN bifurcation. As shown by the eigenvector components in panels (a) and (b) of FIG. 8, the splitting takes place close to the power imbalance border in the Balkans. As before, this mode was initially as in FIG. 2(b) and 2(c). Since the power imbalance is different, the mode evolves differently as well. Nonetheless, the grid splits into two areas when the system reaches instability.

In panel (c), we can see that the line *Paks 380 - San-*

dorfalva 380 is above $\pi/2$ at the threshold of the instability. The second largest phase differences are observed in lines *Brinje 220 - Konjsko 220* and *Ernestinovo 380 - Unlabeled_290 380*, which are at 85.5° and 84.0° respectively. In terms of line stress, we can see in panel (c) that there are a few lines close to their limits. The most loaded lines are *Brinje 220 - Konjsko 220* at 99.7% and *Ernestinovo 380 - Unlabeled_290 380* at 99.5%, followed by *Prijedor 220 - Kakanj 220a* at 96.3% and *Paks 380 - Sandorfalva 380* at 91.6%.

As before, we observe the same splitting in other scenarios as long as they entail large power flows between the Balkans and other regions. In some cases, more than one line goes above $\pi/2$, but the splitting border remains unchanged if we vary the generation distribution within a given area. Moreover, compared to the 2021 scenario [43], we recover the same splitting border in our simulations. Some of the substations involved in the actual incident were Brinje, Ernestinovo, and Prijedor, among others. These substations also stand out in our analysis for having large power flows.

By performing the analysis with the mathematical trick with HVDC lines, we can continue the fixed point from 7.4% to 10.0%, point at which all the lines separating the two regions reach their maximum capacity of 27.72 GW, causing the grid to split into two. In FIG. 9, we show the state of the system at that moment. The red lines shown in panel (d) are the key lines that connect the Balkan region to the rest of the grid. Without them, the area is completely isolated. It is worth noting that these lines are not the minimum set of lines needed to disconnect the two regions.

VI. FINAL DISCUSSION AND CONCLUSION

We have presented a methodology for identifying critical lines in the long-distance transmission in large power grids. Using the European grid as a case study, we examine various scenarios. In particular, we analyze increasingly large interarea flows caused by the large deployment of renewable energies in some regions. As a result, the system loses stability and the grid splits into two asynchronous sub-grids. We observe that the splitting does not necessarily occur at the boundary between the region where generation is increased and the region where it is decreased. In fact, for a broad range of perturbations, splitting takes place either at the Pyrenees or the Balkans.

Similar to the case of the Iberian Peninsula, there are other locations where the geography shapes the topology of the grid. For instance, the Italian Peninsula and Denmark. These locations are susceptible to disruptions for the same reason. Moreover, Sicily is also susceptible to separation from the continental grid given its condition of island and limited connections to mainland. However, in Central Europe, the grid is highly meshed. Hence, the large number of connections decreases vulnerabilities in

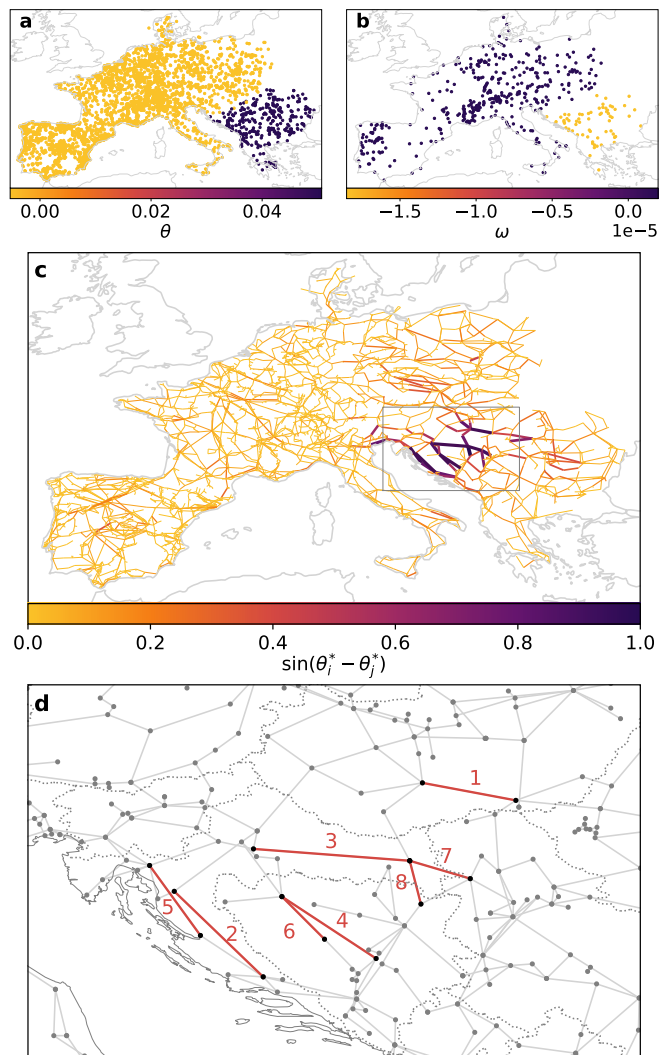


FIG. 9. (a) Phase and (b) frequency components of the eigenvector associated with the eigenvalue that becomes zero; (c) line stress at the threshold of the instability; and (d) lines changed to DC in the splitting region labeled by order of conversion.

this area. Nonetheless, it is still possible to force the system into a splitting situation. Our methodology would allow to find the critical lines between two given regions in such scenarios.

For the cases considered, we find that instabilities occur well after the phase difference in one or more lines is above $\pi/2$. Therefore, line transmission capacity limits are not the immediate cause of the instability. Instead, the instability emerges from a restriction imposed by grid topology. Specifically, it arises from the fact that power transmission through AC lines depends on the phase difference between connecting buses, and sometimes these cannot accommodate the necessary transmission power. Mathematically, the mechanism behind the instability is a pair of complex eigenvalues, associated to a Jacobian eigenvector with non-zero components on nodes with in-

ertia. They become real (Belayakov-Devaney transition) and move apart, triggering a saddle-node bifurcation when one of them becomes 0.

To push the system beyond this limit, we propose a method using HVDC lines. Our strategy involves converting certain lines to DC, which allows us to continue the fixed point further. By doing so, we are able to identify crucial lines in the splitting boundary. These lines are not necessarily the minimum set of lines connecting two given regions. For instance, in the Pyrenees, there are four critical lines and they are the minimum set. However, in the Balkans, we identify eight critical lines, while the minimum set would consist of seven.

Finally we stress that our method – which we applied above to a model of the synchronous grid of continental Europe – is general and can also be applied to identify the most critical lines in other large-scale transmission

grids.

ACKNOWLEDGMENTS

M. Martínez-Barbeito, D. Gomila, and P. Collet acknowledge funding from the European Commission integrated action Virtual Power Plants for Islands, VPP4ISLANDS, (Grant agreement N° 957852), from project APASOS PID2021-122256NB-C22 financed by MCIN/AEI /10.13039/501100011033/ and by EU through FEDER funds, and from Maria de Maeztu program CEX2021-001164-M of MCIN/AEI /10.13039/501100011033/.

J. Fritzsche and P. Jacquod acknowledge funding from the Swiss National Science Foundation under grant 200020.182050.

-
- [1] J. Fleming, *Historical Perspectives on Climate Change* (Oxford University Press, Oxford, England, 1998).
- [2] *Climate Change and Land: an IPCC special report on climate change, desertification, land degradation, sustainable land management, food security, and greenhouse gas fluxes in terrestrial ecosystems*, Tech. Rep. (IPCC, 2019).
- [3] European Commission. Joint Research Centre., *CO2 Emissions of All World Countries :JRC/IEA/PBL 2022 Report*. (Publications Office, LU, 2022).
- [4] C. Fetting, The european green deal, ESDN Report (2020).
- [5] C. A. R. Board, 2022 scoping plan for achieving carbon neutrality, (2022).
- [6] U. D. of State and the US Executive Office of the President, The long-term strategy of the united states, pathways to net-zero greenhouse gas emissions by 2050, (2021).
- [7] I. E. Agency, An energy sector roadmap to carbon neutrality in china, (2021).
- [8] U. Nations, The paris agreement, https://unfccc.int/sites/default/files/resource/parisagreement_publication.pdf (2016).
- [9] D. Heide, L. Von Bremen, M. Greiner, C. Hoffmann, M. Speckmann, and S. Bofinger, Seasonal optimal mix of wind and solar power in a future, highly renewable europe, *Renewable Energy* **35**, 2483 (2010).
- [10] A. S. Anees, Grid integration of renewable energy sources: Challenges, issues and possible solutions, in *2012 IEEE 5th India International Conference on Power Electronics (IICPE)* (IEEE, 2012) pp. 1–6.
- [11] M. A. Basit, S. Dilshad, R. Badar, and S. M. Sami ur Rehman, Limitations, challenges, and solution approaches in grid-connected renewable energy systems, *International Journal of Energy Research* **44**, 4132 (2020).
- [12] X. Liang, Emerging power quality challenges due to integration of renewable energy sources, *IEEE Transactions on Industry Applications* **53**, 855 (2016).
- [13] V. Kumar, A. Pandey, and S. Sinha, Grid integration and power quality issues of wind and solar energy system: A review, in *2016 International conference on emerging trends in electrical electronics & sustainable energy systems (ICETEESES)* (IEEE, 2016) pp. 71–80.
- [14] P. Denholm, T. Mai, R. W. Kenyon, B. Kroposki, and M. O’Malley, *Inertia and the power grid: A guide without the spin*, Tech. Rep. (National Renewable Energy Lab.(NREL), Golden, CO (United States), 2020).
- [15] P. Makolo, R. Zamora, and T.-T. Lie, The role of inertia for grid flexibility under high penetration of variable renewables—a review of challenges and solutions, *Renewable and Sustainable Energy Reviews* **147**, 111223 (2021).
- [16] H. A. Behabtu, M. Messagie, T. Coosemans, M. Berecibar, K. Anlay Fante, A. A. Kebede, and J. V. Mierlo, A review of energy storage technologies’ application potentials in renewable energy sources grid integration, *Sustainability* **12**, 10511 (2020).
- [17] J. Fang, H. Li, Y. Tang, and F. Blaabjerg, On the inertia of future more-electronics power systems, *IEEE Journal of Emerging and Selected Topics in Power Electronics* **7**, 2130 (2018).
- [18] J. Fritzsche and P. Jacquod, A novel adaptive inertia strategy in large-scale electric power grids, arXiv:2311.01350 (2023).
- [19] Q.-C. Zhong and G. Weiss, Synchronverters: Inverters that mimic synchronous generators, *IEEE transactions on industrial electronics* **58**, 1259 (2010).
- [20] F. Monforti, M. Gaetani, and E. Vignati, How synchronous is wind energy production among european countries?, *Renewable and Sustainable Energy Reviews* **59**, 1622 (2016).
- [21] W. Zappa, M. Junginger, and M. Van Den Broek, Is a 100% renewable european power system feasible by 2050?, *Applied energy* **233**, 1027 (2019).
- [22] ENTSOE, Ucte/ucte - the 50 year success story – evolution of a european interconnected grid, https://eepublicdownloads.entsoe.eu/clean-documents/pre2015/publications/ce/110422_UCPTE-UCTE_The50yearSuccessStory.pdf (2003).
- [23] Final report of the investigation committee on the 28 september 2003 blackout in italy, https://eepublicdownloads.entsoe.eu/clean-documents/pre2015/publications/ce/otherreports/20040427_UCTE_IC_Final_r

- eport.pdf (2004).
- [24] J. W. Bialek, Why has it happened again? comparison between the ucte blackout in 2006 and the blackouts of 2003, in *2007 IEEE Lausanne Power Tech* (IEEE, 2007) pp. 51–56.
- [25] C. Li, Y. Sun, and X. Chen, Analysis of the blackout in europe on november 4, 2006, in *2007 International Power Engineering Conference (IPEC 2007)* (IEEE, 2007) pp. 939–944.
- [26] E. Van der Vleuten and V. Lagendijk, Transnational infrastructure vulnerability: The historical shaping of the 2006 european “blackout”, *Energy Policy* **38**, 2042 (2010).
- [27] G. Fotis, V. Vita, and T. I. Maris, Risks in the european transmission system and a novel restoration strategy for a power system after a major blackout, *Applied Sciences* **13**, 83 (2023).
- [28] Eurelectric, Transparency of system operators on cross-border exchange capacities: a survey paper, [https://eepublicdownloads.entsoe.eu/clean-documents/Network codes documents/Implementation/stakeholder_committees/MESC/2020-03-11/5.0 Eurelectric transparency of system operators on cross-border exchange cap.pdf?Web=1](https://eepublicdownloads.entsoe.eu/clean-documents/Network%20codes%20documents/Implementation/stakeholder_committees/MESC/2020-03-11/5.0%20Eurelectric%20transparency%20of%20system%20operators%20on%20cross-border%20exchange%20cap.pdf?Web=1) (2020).
- [29] R. A. Rodriguez, S. Becker, G. B. Andresen, D. Heide, and M. Greiner, Transmission needs across a fully renewable european power system, *Renewable Energy* **63**, 467 (2014).
- [30] L. Pagnier and P. Jacquod, Inertia location and slow network modes determine disturbance propagation in large-scale power grids, *PLoS One* **14**, e0213550 (2019).
- [31] T. Coletta and P. Jacquod, Linear stability and the braess paradox in coupled-oscillator networks and electric power grids, *Physical Review E* **93**, 032222 (2016).
- [32] D. Manik, D. Witthaut, B. Schäfer, M. Matthiae, A. Sorge, M. Rohden, E. Katifori, and M. Timme, Supply networks: Instabilities without overload, *The European Physical Journal Special Topics* **223**, 2527 (2014).
- [33] J. C. Bronski and L. DeVille, Spectral theory for dynamics on graphs containing attractive and repulsive interactions, *SIAM Journal on Applied Mathematics* **74**, 83 (2014).
- [34] M. Fiedler, A property of eigenvectors of nonnegative symmetric matrices and its application to graph theory, *Czechoslovak mathematical journal* **25**, 619 (1975).
- [35] M. Tyloo, L. Pagnier, and P. Jacquod, The key player problem in complex oscillator networks and electric power grids: Resistance centralities identify local vulnerabilities, *Science advances* **5**, eaaw8359 (2019).
- [36] L. Pagnier and P. Jacquod, Pantagruel - a pan-european transmission grid and electricity generation model, <https://zenodo.org/record/2642175#.ZH5B1Bw3E> (2019).
- [37] ENTSOE, Transparency platform, <https://transparency.entsoe.eu>.
- [38] J. Fritzsche and P. Jacquod, Long wavelength coherency in well connected electric power networks, *IEEE Access* **10**, 19986 (2022).
- [39] R. L. Devaney, Reversible diffeomorphisms and flows, *Transactions of the American Mathematical Society* **218**, 89 (1976).
- [40] A. J. Homburg and B. Sandstede, Homoclinic and heteroclinic bifurcations in vector fields, *Handbook of dynamical systems* **3**, 379 (2010).
- [41] ENTSOE, Regional investment plan 2017 continental south west, https://eepublicdownloads.entsoe.eu/clean-documents/tyndp-documents/TYNDP2018/rgip_CSW_Full.pdf (2019).
- [42] I. E. Agency, Energy in the western balkans: The path to reform and reconstruction, <https://iea.blob.core.windows.net/assets/6f3556ba-55bc-4d5b-927c-2d027fd2ebfb/Balkans2008.pdf> (2008).
- [43] I. E. Panel, Continental europe synchronous area separation on 8 january 2021, <https://www.entsoe.eu/news/2021/07/15/final-report-on-the-separation-of-the-continental-europe-power-system-on-8-january-2021/> (2021).